Arabian Journal of Chemistry (2023) **16**, 104889

King Saud University

Arabian Journal of Chemistry

www.ksu.edu.sa
www.sciencedirect.com

ORIGINAL ARTICLE

Dual dynamical jumps on Lie group analysis of hydro-magnetic flow in a suspension of different shapes of water-based hybrid solid particles with Fourier flux

M. Dinesh Kumar [a,1], C.S.K. Raju [a], Mansoor Alshehri [b], Shalan Alkarni [b], Nehad Ali Shah [c,1], Mohamed R. Ali [d,*], R. Sadat [e]

[a] *Department of Mathematics, GITAM School of Science, GITAM, Bangalore 562163, India*
[b] *Department of Mathematics, College of Science, King Saud University, P.O. Box 2455, Riyadh 11451, Saudi Arabia*
[c] *Department of Mechanical Engineering, Sejong University, Seoul 05006, South Korea*
[d] *Faculty of Engineering and Technology, Future University in Egypt, New Cairo 11835, Egypt*
[e] *Department of Mathematics, Faculty of Engineering, Zagazig University, Zagazig, Egypt*

Received 13 November 2022; accepted 4 April 2023
Available online 11 April 2023

KEYWORDS

Fourier Flux;
Cylindrical;
Spherical and Platelet
Hybrid nanofluids;
Velocity slip;
Thermal slip

Abstract In recent times, the mixture of liquids has been referred to as "hybrid modelling." Ternary hybrid models are advantageous for different systems such as production industries, aerosol particle processing, and experimental instrument design, to name a few. The regulating partial differential equation (PDE) for nonlinear systems is changed into a system of associate nonlinear (ODE) In this study, ordinary differential equations report utilizing new similarity scaling symmetry transformations produced via Lie group transformations analysis. Using a BVP4C with a shooting method approach, the resulting system is numerically resolved (MATLAB). For Cases: 1 CNT, Graphene, Aluminium oxide, Cases: 2 Cooper oxide, Magnesium oxide, and Zirconium oxide with different nanosized particle morphologies including platelet, cylindrical, and spherical, the rate of heat transmission and the magnetohydrodynamic flow of incompressible fluid friction were studied. It is observed that Nusselt number transfer is having more transmission rate in case-1 ($Al_2o_3 + GNT + CNT$ with water) than in case-2 ($Mgo + Zro_2 + Cuo\ with\ water$), This shows that,

* Corresponding author.
E-mail addresses: rchakrav@gitm.edu (C.S.K. Raju), mhalshehri@ksu.edu.sa (M. Alshehri), shalkarni@ksu.edu.sa (S. Alkarni), nehadali199@sejong.ac.kr (N.A. Shah), mohamed.reda@fue.edu.eg (M.R. Ali), r.mosa@zu.edu.eg (R. Sadat).
[1] These authors contributed equally to this work and are co-first authors.

Peer review under responsibility of King Saud University.

Production and hosting by Elsevier

https://doi.org/10.1016/j.arabjc.2023.104889

due to the Case-1 hybrid nanofluid mixture's improved heat transmission rate, it can be used for cooling as well as other applications where a faster heat transfer rate is necessary, including rapid charging batteries. Where there is a lower heat transfer rate than in instance 1, the case-2 hybrid nanofluid mixture can be used. Even in cancer treatment also nanoparticles will be useful to kill the cancer cell by injecting the nanoparticles into the human body. In order to predict the outcomes of a response variable, a statistical technique known as multilinear regression analysis (MLR) makes use of a variety of explanatory variables.

Nomenclature

u	Dimensional velocity of the motion in the x-direction (m/s)
a	Stretching rate parameter
v	Dimensional velocity of the motion in the y-direction((m/s)
ρ_{hnf}	Density of the hybrid nanofluid (kg/m3)
μ_{hnf}	hybrid nanofluid's viscosity (Pa. s or kg/ms)
$k_{hnf,}$	The hybrid nanofluid's thermal conductivity(W/mK)
$(\rho c_p)_{hnf}$	The hybrid nanofluid's specific heat(J/kgK)
C_f	Skin friction co-efficient
Nu_x	Local Nusselt number
η	Dimensionless distance parameter
α	slip Parameter for velocity
b	Termal slip coefficient
M	Magnetic number
Q	Heat source/Sink parameter
v	Kinematic viscosity of the fluid $\left(m^2/s\right)$
Pr	Prandtl number
$\varphi = \varphi_1 + \varphi_2 + \varphi_3$	Volume fraction
φ_1	Volume fraction of solid particle-1
φ_2	Volume fraction of solid particle-2
φ_3	Volume fraction of solid particle-3
ψ	Stream function parameter
T, T_∞	Temperature and Free stream temperature
θ	Dimension less temperature

1. Introduction

To eliminate the complications of the model problem, the Lie group analysis is applied by translating PDEs into ODEs. To solve this mathematical method for this model problem will take a long time before using this method. The Lie group transformation is a method for determining partial differential equation symmetry reduction. Lie (Lie, 1891) developed a mechanism for mapping a differential equation. The determining equations are then obtained from a broad infinitesimal group of conversions under which the provided PDEs are unchanged. Pakdemirli (Pakdemirli, 1992) investigated Navier's equation for the boundary layer equation of incompressible fluid flow utilizing the handy coordinate system. The research shows that the border layer equality admits similar clarification when the slope is constant. Pakdemirli and Yurusoy (Pakdemirli and Yurusoy, 1998) investigated the significance of similarity conversions and their applications in PDE. Many academics expanded on Pakdemirli and Yurusoy's (Pakdemirli and Yurusoy, 1998) work to look into different flow scenarios (Mukhopadhyay et al., 2005; Sivasankaran et al., 2006). Many have studied the influence of nonlinear and linear slip on the hydrodynamic changes on a boundary layer over various geometric configurations. Martin and Boyd (Martin and Boyd, 2006; Martin and Boyd, 2010) are some of the authors. Changes in the heat source, viscoelastic behaviour, radiation, buoyancy, magnetohydrodynamic effects, and thermal conductivity in the fluid were all considered by Abel and Mahesha et al. (Abel et al., 2009). Aziz and Abdul (Aziz, 2010) investigated the hydrodynamic and thermic slide flow border layers on a horizontal plate with fixed heat changes at border conditions. He finally says that as the slide parameter-specific value rises, the slide velocity raises, and at the fence, shear stress falls. Aziz (Aziz, 2009) newly applied the convection edge condition. Slip flow and convective boundary conditions have been studied on boundary layers with varying diffusivity analysed by Hamad et al. (Investigation of combined heat and mass transfer, 2012). Due to its significance in medical sciences and bioengineering, such as the targeted transmission of drugs using magneto pieces as drug carriers, Magneto Resonance imagination for imaging, and treatment of cancer tumours causes magneto hyperthermia by Misra et al. (Misra et al., 2010), A bio-magnetic liquid's edge layer flow and heat transmission across a contracting or elastic sheet has been extensively investigated over the past decades. Researchers have been studying the Heat-physical features of non-Newtonian fluids in several sciences and engineering disciplines. Chemical, pharmaceutical, and other industrial sectors can use these fluids. However, learning non-Newtonian fluids is a challenging subject. Due to their heterogeneous nature, very nonlinear governing equations exist compared to equations for Newtonian fluids and one constitutive equation that explicitly represents them. Researchers have proposed various basic formulas for analysing the physical characteristics of in light of these worries, non-Newtonian fluids. Tangent hyperbolic fluid is a non-Newtonian model used in various industrial operations and laboratory research. Various academics have looked at the hyperbolic tangent model from multiple angles (Friedman et al., 2013; Naseer et al., 2014; Azhar et al., 2017; Salahuddin et al., 2017).

Nanoparticles range in size from 0 to 100 nm. HNF composite non-metallic, metallic, or polymeric nano-sized power and the base fluid are used to optimize heat transmit rates in various applications. The suspension of a nano-sized solid phase in a liquid can significantly boost thermal conductivity, a beneficial modification for enhancing heat transfer analysed by Ahmadi et al. (Ahmadi et al., 2018). The hybrid nanofluids outperformed the base fluid and comparable nanofluids in terms of thermal performance. Other investigations have demonstrated that binary hybrid nanofluids have improved thermo-physical properties compared to single nanofluids (Huminic and Huminic, 2020; Soltani et al., 2020), Reddy et al. (Reddy et al., 2020) present several hybrid applications. The performance of the reproduced HMX is investigated by Kashyap et al. (Kashyap et al., 2021), utilizing different water-based HNFs as coolants and surface changes. (Fin, groove, Capsule embossing). First, different hybrid nanofluids were used to compare the version of regenerative HMX (exergy efficiency, humidity point efficacy, and cooling capacity). The water consumption rate and other parameters were then determined by altering the operating parameters between various cooling plate surface modifications (coolant flow rate, air inlet velocity, and inlet dew-point depression). Lengthwise no loss of mass and energy in the channels is employed for each differential equation element. Numerous industrial applications are included in the potential uses for these nanofluids with improved heat transmittance performance as reported by Younes et al. (Younes et al., 2022). Gas mileage improvements and advancements in nuclear reactor cooling systems may result from enhanced performance of pumps, lighter radiators, micro-electronics systems, and other auto parts.

Analysis of a stretchable spinning system with a heat source and sink's thermal and entropy generation, Heat generation and nonlinear radiation effects on MHD Casson nanofluids were seen across a thin needle submerged in a porous medium. Effects of Nanoparticles on Fluid Heat Transfer Through Porous Channel Due to Geometry and Shape, Thermal Performance Assessment of MHD Nanofluid Transport in a Rotating System Undergoing Uniform Injection/Suction and Heat Generation, Akinshilo et al. (Akinshilo et al., 2022; Akinshilo et al., 2021; Akinshilo, 2019; Akinshilo, 2020; Mabood and Akinshilo, 2021; Akinshilo et al., 2020) have studied the stability analysis and heat transfer of hybrid Cu-Al2O3/H2O nanofluids as they pass through a stretched surface using Jeffery Hamel's diverging/converging channel heat transfer analysis. Bioconvective Slip Flow of Radiated Magneto-Cross-Nanomaterial Over Stretching Cylinder/Plate with Activation Energy: Asgar Ali et al. (Ali et al., 2021). investigation on the Cattaneo-Christov double diffusions theory Over an inclined exponentially extending surface, By Das et al. (Das et al., 2021), Darcy-Forchheimer flow of a magneto-radiated pair stress fluid with Ohmic dissipation. Sarkar et al. (Sarkar et al., 2020) conducted an entropy research to determine how activation energy affected the flow of radiated magneto-Sisko nanofluid over a stretching and slipping cylinder. Das et al. (Das et al., 2017) described a magneto-nanofluid second-order slip flow along a stretching cylinder with a prescribed heat flux. Makinde et al. (Makinde et al., 2016) described the Navier Slip Effects on Chemically Reacting Nanofluid in MHD Over a Convective Permeable Surface with Radiative Heat. Interesting and recent results considered the effect of magnetohydrodynamic are (Sajjan et al., 2022; Raza et al., 2022; Abderrahmane et al., 2022; Rasool et al., 2023; Shah et al., 2023).

After carefully examining the aforementioned literature, it was found that no literature had ever taken into account the impact of dynamical jumps and Fourier fluxes on Lie group transformation. Considering the dual dynamical leaps on Lie group analysis of hydro-magnetic flow in a suspension of various shaped water-based hybrid solid particles with Fourier flux, one can take this into account.

2. Modelling and Formulation:

A continuous, two-dimensional flow of a tangent hyperbolic fluid is incompressible. The liquid at $y = 0$ is parallel to the plane, which restricts the flow through the area. At $y > 0$. We also think fluid generation is caused by linear stretching.

The liquid's Shear stress is given by (Akbar et al., 2012).

$$\bar{\tau} = \left[\mu_\infty + (\mu_0 + \mu_\infty)\tanh\left(\Gamma\bar{\dot{\gamma}}\right)^n\right]\bar{\dot{\gamma}}. \tag{1}$$

It varies based on time material fixed value, flow behaviour index, excess stress tensor, zero shear rate and infinite shear rate viscosities, and zero shear rate are all denoted by $\bar{\tau}$, μ_0, μ_∞, Γ, and n. $\bar{\dot{\gamma}}$ $\bar{\dot{\gamma}}$ is the first letter of the

$$\bar{\dot{\gamma}} = \sqrt{\frac{1}{2}\sum_i\sum_j \bar{\dot{\gamma}}_{ji}\bar{\dot{\gamma}}_{ij}} = \sqrt{\frac{1}{2}\Pi} \tag{2}$$

In collaboration with $\Pi = \frac{1}{2}tr\left[\left((gradV^T) + gradV\right) * \left((gradV^T) + gradV\right)\right]$.

Considering the case $\mu_\infty = 0$ because we used an infinite shear rate viscosity in the ones below. We must take it $\Gamma\bar{\dot{\gamma}} < 1$ then being looked into the definition of shear stress is as follows:

Then Eq. (1) becomes

$$\bar{\tau} = \mu_0\left[\left(\Gamma\bar{\dot{\gamma}}\right)\right]\bar{\dot{\gamma}} = \mu_0\left[\left(1 + \Gamma\bar{\dot{\gamma}} - 1\right)^n\right]\bar{\dot{\gamma}},$$

$$= \mu_0\left[1 + n\left(\Gamma\bar{\dot{\gamma}} - 1\right)\right]\bar{\dot{\gamma}}. \tag{3}$$

The Governing equations has been defined as follows by using the studies (Akbar et al., 2012; Ullah and Zaman, 2017) and Akbar et al. (Akbar et al., 2013)

$$\frac{\partial\bar{v}}{\partial\bar{y}} + \frac{\partial\bar{u}}{\partial\bar{x}} = 0 \tag{4}$$

$$\rho_{hnf}\left(\bar{u}\frac{\partial\bar{u}}{\partial\bar{x}} + \bar{v}\frac{\partial\bar{u}}{\partial\bar{y}}\right) = \mu_{hnf}\frac{\partial^2\bar{u}}{\partial\bar{y}^2} - \sigma B^2\bar{u} \quad 5)$$

$$\left(\rho c_p\right)_{hnf}\left(\bar{u}\frac{\partial T}{\partial\bar{x}} + \bar{v}\frac{\partial T}{\partial\bar{y}}\right) = K_{hnf}\frac{\partial^2 T}{\partial\bar{y}^2} + Q_0(T - T_\infty) \tag{6}$$

Liquid density and kinematic liquid viscosity are represented by ρ, υ the velocity u, v in the direction y, x, respectively. The uniform magnetic field B that has been applied,The word refers to the liquid electrical conductivity σ and the fluid's specific heat value is c_p, k stand for thermal conduction, and heat generating parameter is Q_0, respectively. Temperature quantities for free stream and temperature quantities are T and T_∞.

The conditions for the boundary are given by

$$For\, y = 0,\ T = T_w + D_1\frac{\partial T}{\partial y}, u = L\frac{\partial u}{\partial y} + ax, v = 0. \tag{7}$$

$$For\, u \to 0, T \to T_\infty, y \to \infty \tag{8}$$

The stretching rate is a, the velocity slip factor is L, and the thermal slip factor is $D_1(x)$. The no-slip condition has been restored $L = 0 = D_1(x)$.

The offered non-dimensional system is where we should start. For this, we offer the non-dimensional quantities below.

$$\theta = \frac{T - T_\infty}{T_w - T_\infty}, \bar{x} = \sqrt{\frac{v}{a}}x, \bar{u} = \sqrt{av}u, \bar{y} = \sqrt{\frac{v}{a}}y, \bar{v} = \sqrt{av}v. \tag{9}$$

When the one bar is removed from the system described by Equations (4)-(6), the energy, momentum, and continuity equations transform into

$$\frac{\partial v}{\partial y} + \frac{\partial u}{\partial x} = 0 \tag{10}$$

$$\rho_{hnf}\left(v\frac{\partial u}{\partial y} + u\frac{\partial u}{\partial x}\right) = \mu_{hnf}\frac{\partial^2 u}{\partial y^2} - \frac{\sigma B^2}{a}u \tag{11}$$

$$\left(\rho c_p\right)_{hnf}\left(u\frac{\partial T}{\partial x} + v\frac{\partial T}{\partial y}\right) = K_{hnf}\frac{\partial^2 T}{\partial y^2} + Q_0(T - T_\infty) \tag{12}$$

The scaling scenario given in (9), has the following boundary conditions by using (7) and (8) equations:

$$For\, y = 0, u = \sqrt{\frac{a}{v}}L\frac{\partial u}{\partial y} + x, \theta = 1 + \sqrt{\frac{a}{v}}D_1\frac{\partial \theta}{\partial y}. \tag{13}$$

$$For\, y \to \infty, \theta \to 0, u \to \infty. \tag{14}$$

Streaming functionality $v = -\frac{\partial \psi}{\partial \bar{x}}$ and $u = \frac{\partial \psi}{\partial \bar{y}}$ it is employed to reduce the Non-dependent inconstant and equations. Equation (10), as well as Equations (12) & (13), are satisfied (11),are representing in the form of stream functions ψ and as follows.

$$\rho_{hnf}\left(\frac{\partial^2\psi}{\partial x\partial y}\frac{\partial\psi}{\partial y} - \frac{\partial^2\psi}{\partial y^2}\frac{\partial\psi}{\partial x}\right) = \mu_{hnf}\frac{\partial^3\psi}{\partial y^3} - \frac{\sigma B^2}{a}\frac{\partial\psi}{\partial y} \tag{15}$$

$$\left(\frac{\partial\psi}{\partial y}\frac{\partial\theta}{\partial x} - \frac{\partial\psi}{\partial x}\frac{\partial\theta}{\partial y}\right) = \frac{K_{hnf}}{(\mu c_p)_{hnf}}\frac{\partial^2\theta}{\partial y^2} + \frac{Q_0\theta}{(\rho c_p)_{hnf}a} \tag{16}$$

The boundary conditions (13) and (14) are translated to by the stream function's induction.

$$\theta = 1 + D_1\sqrt{\frac{a}{v}}\frac{\partial\theta}{\partial y}, \frac{\partial\psi}{\partial x} = 0, \frac{\partial\psi}{\partial y} = x + \sqrt{\frac{a}{v}}L\frac{\partial^2\psi}{\partial y^2}\, for\, y = 0. \tag{17}$$

$$\theta \to 0, \frac{\partial\psi}{\partial y} \to 0\, for\, y \to \infty. \tag{18}$$

2.1. Analysis:

In this part, we create new similarity rules for Equations (15) and using Lie group analysis (16). We shall convert the nonlinear PDE to a nonlinear ODE. For this, we assess the following transformation scaling group.

$$\Gamma : \Gamma^* = \psi^* = e^{\varepsilon\gamma_3}\psi, \Gamma e^{\varepsilon\gamma_5}, \theta^* = e^{\varepsilon\gamma_4}\theta, x^* = xe^{\varepsilon\gamma_1}, y^* = ye^{\varepsilon\gamma_2}. \tag{19}$$

Then, Group γ_i and Γ ,for the values of $(i = 1, 2, 3, 4, 5)$ regarding the specification of parameter, ε are the real value need to find. Point transformation is used to transform the coordinates. $(\bar{x}, \bar{y}, \psi, \theta, \Gamma)$ to $(\bar{x}^*, \bar{y}^*, \psi^*, \theta^*, \Gamma^*)$ by (19).

By entering it into Equations (15) and (19), we obtain (16).

$$e^{\varepsilon(\gamma_1+2\gamma_2-2\gamma_3)}\rho_{hnf}\left(\frac{\partial^2\psi^*}{\partial x^*\partial y^*}\frac{\partial\psi^*}{\partial y^*} - \frac{\partial^2\psi^*}{\partial y^{*2}}\frac{\partial\psi^*}{\partial x^*}\right) = \mu_{hnf}e^{\varepsilon(3\gamma_2-\gamma_3)}\frac{\partial^3\psi^*}{\partial y^{*3}} - e^{\varepsilon(\gamma_2-\gamma_3)}\frac{\sigma B^2}{a}\frac{\partial\psi^*}{\partial y^*} \tag{20}$$

$$e^{\varepsilon(\gamma_1+\gamma_2-\gamma_3-\gamma_4)}\left(\frac{\partial\theta^*}{\partial x^*}\frac{\partial\psi^*}{\partial y^*} - \frac{\partial\theta^*}{\partial y^*}\frac{\partial\psi^*}{\partial x^*}\right) = \frac{K_{hnf}}{(\mu c_p)_{hnf}}e^{\varepsilon(-\gamma_4+2\gamma_2)}\frac{\partial^2\theta^*}{\partial y^{*2}} + e^{-\varepsilon\gamma_4}\frac{Q_0\theta^*}{(\rho c_p)_{hnf}a} \tag{21}$$

The modified systems (20) and (21), when subjected to the group of transformations, will not change if the coefficients of the aforementioned equations are equivalent.

$$\gamma_1 + 2\gamma_2 - 2\gamma_3 = 3\gamma_2 - \gamma_3 = \gamma_2 - \gamma_3 \tag{22}$$

$$\gamma_1 + \gamma_2 - \gamma_3 - \gamma_4 = 2\gamma_2 - \gamma_4 = -\gamma_4 \tag{23}$$

From the boundary condition, we have the following

$$\gamma_4 = 0 \tag{24}$$

We combine the solutions to Eqs. (22) and (23) to obtain.

$$\gamma_1 = \gamma_3, \gamma_2 = 0, \gamma_3 = \gamma_1, \gamma_4 = 0. \tag{25}$$

By integrating (25) the transformation into the scaling, the following single-parameter group of modifications are created (19).

$$\Gamma : x^* = xe^{\varepsilon\gamma_1}, y^* = y, \psi^* = \psi e^{\varepsilon\gamma_1}, \theta = 0. \tag{26}$$

The following condensed form is created by adding Taylor's series to the 26′s one-parameter group while keeping the terms up to order ε.

$$y^* = y, \psi^* - \psi = x\varepsilon\gamma_1, x^* = x + x\varepsilon\gamma_1, \theta^* - \theta = 0. \tag{27}$$

Eq. makes it simple to represent the collection of transformations as characteristic equations (27).

$$\frac{dx}{x\gamma_1} = \frac{d\theta}{0} = \frac{dy}{0} = \frac{d\psi}{x\gamma_1} \tag{28}$$

Eqs contain the similarity transformations (28). We get $\frac{dx}{x\gamma_1} = \frac{dy}{0}$ Eq. (28), who's initial two terms we can combine to get

$$y = \eta\,(say) constant. \tag{29}$$

By using 3,1 terms to produce Eq. (28) yields $\frac{d\psi}{x\gamma_1} = \frac{dx}{x\gamma_1}$.

$$\frac{\psi}{x} = constant = f(\eta)\,(say),\ then\, \psi = xf(\eta) \tag{30}$$

Equating the 1st and 4th terms and integrating both sides of Equation (28) yields

$$\theta = \theta(\eta). \tag{31}$$

The new similarity transformations as a result

$$\eta = y, \psi = xf(\eta), \theta = \theta(\eta). \tag{32}$$

In light of this, the new similarity transformations by putting Eqs (32) in (15) & (16).

$$f'''(\eta)\frac{\mu_{hnf}}{\rho_{hnf}} - f(\eta)M^2 - (f'(\eta))^2 + f(\eta)f''(\eta) = 0 \tag{33}$$

$$\left(\frac{k_{hnf}}{(\mu c_p)_{hnf}}\right)\theta''(\eta) + f(\eta)\theta'(\eta) + Q\theta(\eta) = 0 \tag{34}$$

It is the Prandtl numeral $\Pr = \frac{\mu c_p}{k}$, source/sink is a parameter $Q = \frac{Q_0}{\rho c_p a}$, and the parameter for the source/sink is $M^2 = \frac{\sigma B^2}{\rho a}$.

Differentials utilising η are represented by primes. We solve the problem using Eqs. (33) and (34) subject to the border conditions being (34).

$$For\,\eta \to 0, \frac{d}{d\eta}(f(0)) = \alpha f''(0) + 1, f(0) = 0, \theta(0) = b\theta'(0) + 1. \tag{35}$$

$$For\,\eta \to \infty, f'(\infty) \to 0, \theta(\infty) \to 0. \tag{36}$$

It is the velocity slip. $\alpha = \sqrt{\frac{a}{v}}L$, even though the thermal slip is $b = \sqrt{\frac{a}{v}}D_1$ in the equations above.

The Nu_x and C_f are defined.

$$\frac{\tau_w}{\rho(a\bar{x})^2} = C_f, \frac{\bar{x}q_w}{k(T_w - T_\infty)} = Nu_x \tag{37}$$

The coefficient of Nu_x and C_f are defined.

$$\mu\left(\frac{\partial \bar{u}}{\partial \bar{y}}\right)_{\eta=0} = \tau_w, -k\left(\frac{\partial T}{\partial \bar{y}}\right)_{\eta=0} = q_w. \tag{38}$$

The local Nu_x and C_f lose their dimension when Eqs. (9) and (32) are placed into equation (37).

$Re^{\frac{1}{2}}Cf = f''(0), Re^{-\frac{1}{2}}Nu_x = -\theta'(0)$. Represents the Reynolds number.

The following are some applications of hybrid nanofluid thermophysical properties:

The Solid particle-1 Platelet (Al_2O_3), cylindrical (GNT), spherical (CNT), and platelet (magnesium oxide) nanoparticles are represented by the volume φ_1, φ_2 and φ_3. Solid particle-2 Spherical (Copper oxide), cylindrical (Zirconium oxide), and platelet nanoparticle volume fraction nanoparticles are represented by $\varphi = \varphi_1 + \varphi_2 + \varphi_3$. The viscosity and heat conductivity of THNF particles (spherical, cylindrical, platelet, and shapes) are

$$\mu_{hnf} = (\varphi^{-1}\mu_{nf3}\varphi_3 + \varphi^{-1}\mu_{nf1}\varphi_1 + \varphi^{-1}\mu_{nf2}\varphi_2) \tag{39}$$

$$k_{hnf} = (\varphi^{-1}k_{nf1}\varphi_1 + \varphi^{-1}k_{nf2}\varphi_2 + \varphi^{-1}k_{nf3}\varphi_3) \tag{40}$$

The density ρ_{hnf} of spherical, cylindrical, platelet ternary hybrid nanoparticles is given by

$$\rho_{hnf} = \varphi_1\rho_{\mathrm{sp1}} + \varphi_3\rho_{\mathrm{sp3}} + \varphi_2\rho_{\mathrm{sp2}} + (1-\varphi_1-\varphi_2-\varphi_3)\rho_{\mathrm{bf}} \tag{41}$$

The $(\rho c_p)_{hnf}$ heat capacity of ternary hybrid nanoparticles is estimated using the following formulas:

$$(\rho c_p)_{hnf} = (1-\varphi_1-\varphi_2-\varphi_3)(\rho \mathrm{c_p})_{\mathrm{bf}} + \varphi_3(\rho \mathrm{c_p})_{\mathrm{sp3}} + \varphi_2(\rho \mathrm{c_p})_{\mathrm{sp2}} + \varphi_1(\rho \mathrm{c_p})_{\mathrm{sp1}} \tag{42}$$

Spherical nanoparticles have the following viscosity and thermal conductivity:

$$\mu_{nf1} = (\mu_{bf})(6.2\varphi^2 + 2.5\varphi + 1) \tag{43}$$

$$\frac{k_{nf1}}{k_{bf}} = \left[\frac{(-2\varphi k_{bf} + 2\varphi \mathrm{k_{sp1}}) + 2\mathrm{k_{bf}} + \mathrm{k_{sp1}}}{(-\varphi \mathrm{k_{sp1}} + \varphi \mathrm{k_{bf}}) + \mathrm{k_{sp1}} + 2\mathrm{k_{bf}}}\right] \tag{44}$$

The viscosity and heat conductivity of cylindrical nanoparticles are:

$$\frac{\mu_{nf2}}{\mu_{bf}} = \left(1 + 13.5\varphi + 904.4\varphi^2\right) \tag{45}$$

$$\frac{k_{nf2}}{k_{bf}} = \left[\frac{-3.9(\varphi \mathrm{k_{bf}} - \varphi \mathrm{k_{sp2}}) + \mathrm{k_{sp2}} + 3.9\mathrm{k_{bf}}}{(\varphi \mathrm{k_{bf}} - \varphi \mathrm{k_{sp2}}) + 3.9\mathrm{k_{bf}} + \mathrm{k_{sp2}}}\right] \tag{46}$$

The platelet nanoparticles' thermal conductivity and thermal viscosity are as follows:

$$\frac{\mu_{nf3}}{\mu_{bf}} = \left(1 + 37.1\varphi + 612.6\varphi^2\right) \tag{47}$$

$$\frac{k_{nf3}}{k_{bf}} = \left[\frac{4.7k_{bf} + k_{sp3} - 4.7(\varphi \mathrm{k_{bf}} - \varphi \mathrm{k_{sp3}})}{k_{sp3} + 4.7k_{bf} + (\varphi \mathrm{k_{bf}} - \varphi \mathrm{k_{sp3}})}\right] \tag{48}$$

The eqns (34) and (33)'s aforementioned properties are below.

$$\left(\frac{A_1}{A_2\varphi}\right)f'''(\eta) + f(\eta)f''(\eta) - (f'(\eta))^2 - M^2 f(\eta) = 0 \tag{49}$$

$$\left(\frac{A_4}{A_3}\right)(\Pr\varphi)\theta''(\eta) + f(\eta)\theta'(\eta) + Q\theta(\eta) = 0 \tag{50}$$

The transformations in the equations above are as follows.

$$A_1 = \varphi_3 \mathrm{B}_3 + \varphi_2 \mathrm{B}_2 + \varphi_1 \mathrm{B}_1$$

$$A_2 = 1 - \varphi_1 - \varphi_2 - \varphi_3 + \varphi_1\frac{\rho_{\mathrm{sp1}}}{\rho_{\mathrm{bf}}} + \varphi_2\frac{\rho_{\mathrm{sp2}}}{\rho_{\mathrm{bf}}} + \varphi_3\frac{\rho_{\mathrm{sp3}}}{\rho_{\mathrm{bf}}}$$

$$A_3 = B_4\varphi_1 + \mathrm{B}_5\varphi_2 + \mathrm{B}_6\varphi_3$$

$$A_4 = \varphi_1\frac{(\rho \mathrm{c_p})_{\mathrm{sp1}}}{(\rho \mathrm{c_p})_{\mathrm{bf}}} + \varphi_2\frac{(\rho \mathrm{c_p})_{\mathrm{sp2}}}{(\rho \mathrm{c_p})_{\mathrm{bf}}} + \varphi_3\frac{(\rho \mathrm{c_p})_{\mathrm{sp3}}}{(\rho \mathrm{c_p})_{\mathrm{bf}}} + 1 - \varphi_1 - \varphi_2 - \varphi_3$$

$$A_5 = (1-\varphi_1-\varphi_2-\varphi_3) + \varphi_1\frac{(\rho\beta_0)_{\mathrm{sp1}}}{(\rho\beta_0)_{\mathrm{bf}}} + \varphi_2\frac{(\rho\beta_0)_{\mathrm{sp2}}}{(\rho\beta_0)_{\mathrm{bf}}} + \varphi_3 \times \frac{(\rho\beta_0)_{\mathrm{sp3}}}{(\rho\beta_0)_{\mathrm{bf}}}$$

$$A_6 = (1-\varphi_1-\varphi_2-\varphi_3) + \varphi_1\frac{(\rho\beta_1)_{\mathrm{sp1}}}{(\rho\beta_1)_{\mathrm{bf}}} + \varphi_2\frac{(\rho\beta_1)_{\mathrm{sp2}}}{(\rho\beta_1)_{\mathrm{bf}}} + \varphi_3 \times \frac{(\rho\beta_1)_{\mathrm{sp3}}}{(\rho\beta_1)_{\mathrm{bf}}}$$

$$B_1 = 6.2\varphi^2 2.5\,\varphi + 1$$

$$B_2 = 904.4\varphi^2 + 13.5\,\varphi + 1$$

$$B_3 = 612.6\varphi^2 + 37.1\,\varphi + 1$$

$$B_4 = \frac{k_{sp1} + 2k_{bf} - 2\varphi(k_{bf} - k_{sp1})}{k_{sp1} + 2k_{bf} + \varphi(\mathrm{k_{bf}} - \mathrm{k_{sp1}})}$$

$$B_5 = \frac{3.9k_{bf} + k_{sp2} + (-3.9\varphi k_{bf} + 3.9\varphi k_{sp2})}{3.9k_{bf} + k_{sp2} + (\varphi \mathrm{k_{bf}} - \varphi \mathrm{k_{sp2}})}$$

$$B_6 = \frac{k_{sp3} + 4.7k_{bf} - 4.7\varphi(k_{bf} - k_{sp3})}{k_{sp3} + 4.7k_{bf} + \varphi(\mathrm{k_{bf}} - \mathrm{k_{sp3}})}$$

3. Methodology:

3.1. Principle of Homogeneity:

$$\frac{\partial v}{\partial y} + \frac{\partial u}{\partial x} = 0 \ (Continuity\ equation)$$
$$\frac{m}{sm} + \frac{m}{sm} = 0$$
$$\frac{1}{s} + \frac{1}{s} = 0$$
$$\rho_{hnf}\left(v\frac{\partial u}{\partial y} + u\frac{\partial u}{\partial x}\right) = \mu_{hnf}\frac{\partial^2 u}{\partial y^2} - \frac{\sigma B^2}{a}u \ (Momentum\ equation)$$
$$\frac{m}{s}\frac{m}{sm} + \frac{m}{s}\frac{m}{sm} = \frac{kgs^{-1}m^{-1}}{kgm^{-3}}\frac{ms^{-1}}{m^2} - \frac{ms^{-1}\left(kg^{-1}m^{-3}c^2s\right)\left(kg^2s^{-2}c^{-2}\right)}{kgm^{-3}}$$
$$\frac{m}{s^2} + \frac{m}{s^2} = \frac{m}{s^2} - \frac{m}{s^2}$$
$$(\rho c_p)_{hnf}\left(u\frac{\partial T}{\partial x} + v\frac{\partial T}{\partial y}\right) = K_{hnf}\frac{\partial^2 T}{\partial y^2} + Q_0(T - T_\infty) \ (Energy\ equation)$$
$$\frac{ms^{-1}k}{m} + \frac{ms^{-1}k}{m} = \frac{kgs^{-3}mk^{-1}}{kgm^{-1}s^{-2}k^{-1}}\frac{k}{m^2} + \frac{kgs^{-4}m^2k^{-1}}{kgs^{-3}m^2k^{-1}}$$
$$\frac{k}{s} + \frac{k}{s} = \frac{k}{s} + \frac{k}{s}$$

This helps to confirm the provided model is correct and can move further.

3.2. Numerical Method:

The changed equations (49–50) are resolved using MATLAB's built-in function BVP4C in light of the circumstances (35–36). We solve this problem using the BVP4C solver since it is a built-in function (Mamatha and Raju (Upadhya and Raju, 2022).

To take this into account, we used the Runge-Kutta method along with the BVP4C solver.

Before beginning the coding process, we make the below assumptions.

$f = g_1, f\prime = g_2, f\prime\prime = g_3, \theta = g_4, \theta\prime = g_5.$

The following equations and conditions can be used to construct a first-order system of ODEs:

$$\left.\begin{array}{c} g_1' = g_2 \\ g_2' = g_3 \\ g_3' = \varphi\left(\frac{A_2}{A_1}\right)\left[(g'(\eta))^2 + M^2 g'(\eta) - g''(\eta)g(\eta)\right] \\ g_4' = g_5 \\ g_5' = \Pr\varphi\left(\frac{A_4}{A_3}\right)[-g(\eta)\theta\prime(\eta) - Q\theta(\eta)] \end{array}\right\}$$

considering the situation

$$\left.\begin{array}{c} f_d(2) = 0 \\ f_d(4) = 0 \\ f_c(4) = 1 + bf_c(5) \\ f_c(1) = 0 \\ f_c(2) = 1 + \alpha f_c(3) \end{array}\right\}$$

To analyse the correlation between the various parameters for the outcome solution, multilinear regression (MLR) is used.

Skin friction for the parameters $\varphi, \varphi_1, \varphi_2, \varphi_3, \alpha, M$..

$$Skn_{Case-1} = 54.7123\varphi + 0\varphi_1 + 0\varphi_2 + 66.7669\varphi_3 - 68.6057M - 40.5983\alpha + 9.406425.$$
$$Skn_{Case-2} = 45.6768\varphi + 0\varphi_1 - 1.39879\varphi_2 + 0\varphi_3 - 10.3454M + 4.944414\alpha + 6.752391.$$
$$Skn_{Case-3} = 0\varphi + 0\varphi_1 + 41.70733\varphi_2 + 13.32583\varphi_3 - 5.87046M - 1.08838\alpha + 2.464384.$$

Nusselt number for the parameters $\varphi, \varphi_1, \varphi_2, \varphi_3, b, \Pr$

$$Nus_{Case-1} = 3.49911\varphi + 0\varphi_1 - 1.25087\varphi_2 + 0\varphi_3 - 0.49167\Pr + 1.06948b - 11.1207.$$
$$Nus_{Case-2} = 0\varphi + 0.011843\varphi_1 - 0.31437\varphi_2 + 0.665228\varphi_3 + 1.213388\Pr + 0b - 7.84828.$$
$$Nus_{Case-3} = 0\varphi + 0\varphi_1 + 0.262608\varphi_2 - 0.32438\varphi_3 + 0.443118\Pr + 0.315568b - 2.13053.$$

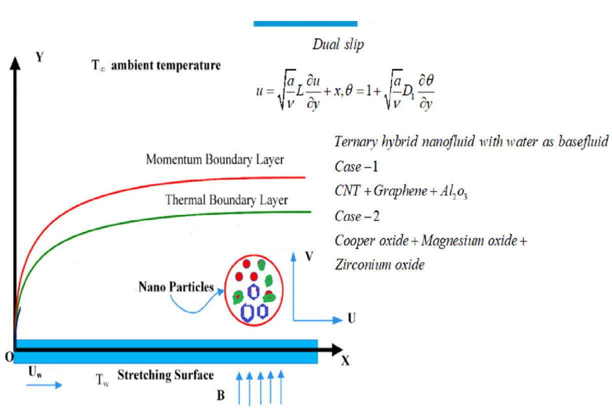

Fig. 1 Physical model.

4. Results analysis and Discussion:

4.1. Multi-Linear regression analysis:

The effects of utilising 3-D surface plots with multilinear

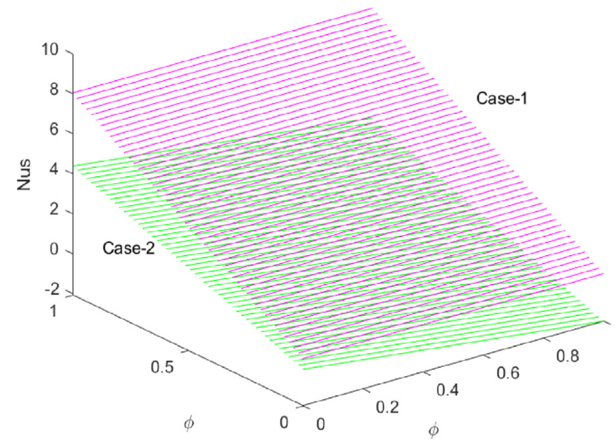

Fig. 2 The effect of φ and φ_1 on Nus.

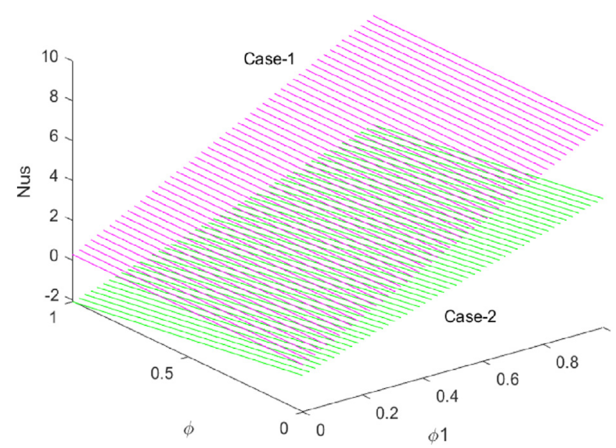

Fig. 3 The effect of φ_1 and φ on Nus.

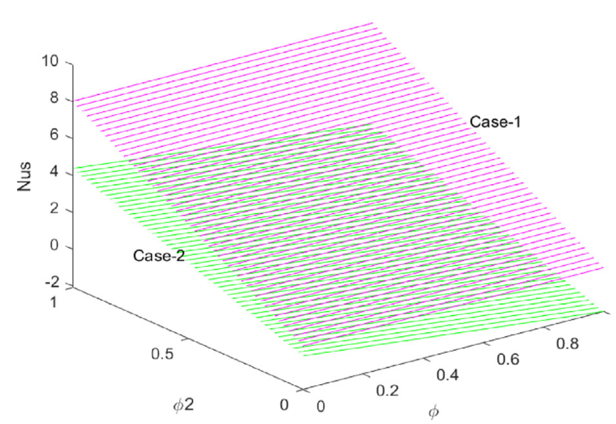

Fig. 4 The effect of φ and φ_2 on Nus.

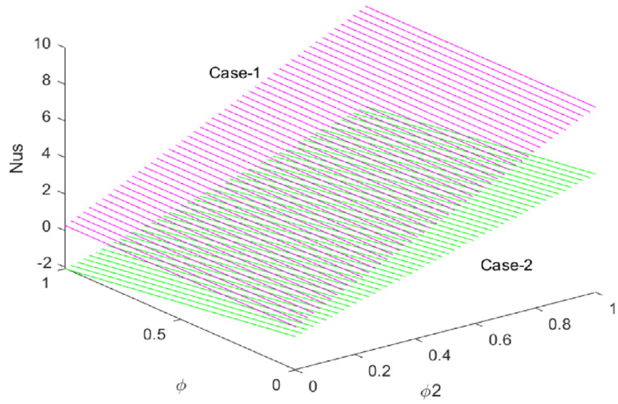

Fig. 5 The effect of φ_2 and φ on Nus.

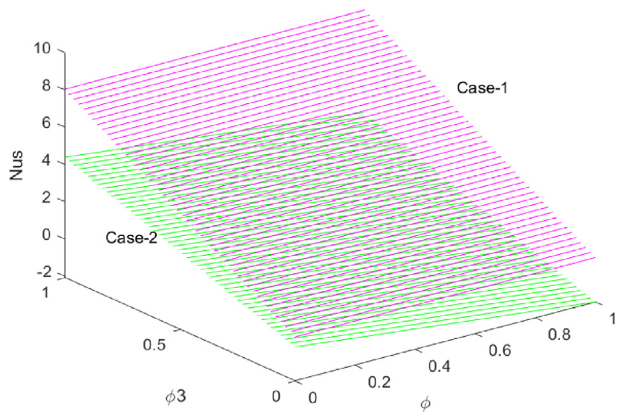

Fig. 6 The effect of φ and φ_3 on Nus.

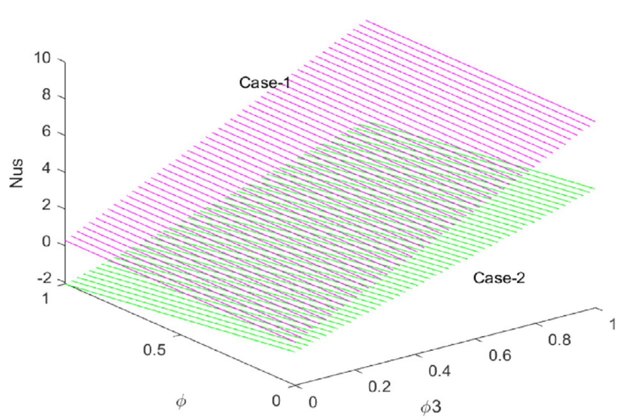

Fig. 7 The effect of φ_3 and φ on Nus.

regression to analyse the $\varphi, \varphi_1, \varphi_2, \varphi_3, b, \mathrm{Pr}$ on Nu_x from Figs. 1-8 and the effect of $\varphi, \varphi_1, \varphi_2, \varphi_3, \alpha, M$ on C_f from Figs. 1-16. A regression line is present. $R = D_1X_1 + D_2X_2 + D_3X_3$......, the slope of regression is an independent property. Here, the following two instances are explored.

Skin friction and Nusselt number multi-linear regression data are presented as.

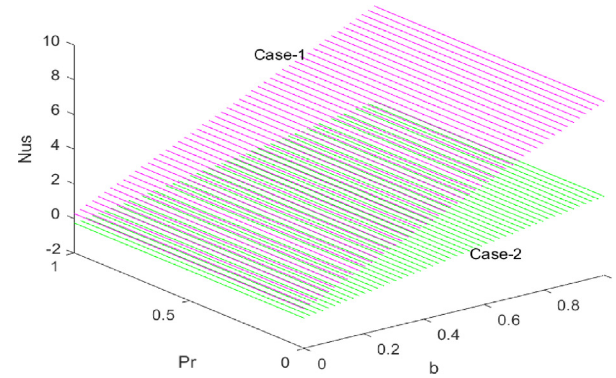

Fig. 8 The effect of b and Pr on Nus.

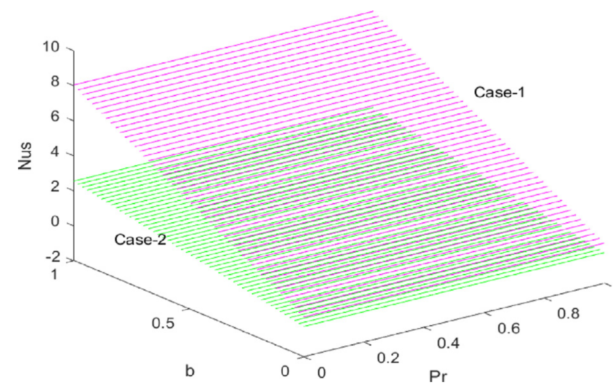

Fig. 9 The effect of Pr and b on Nus.

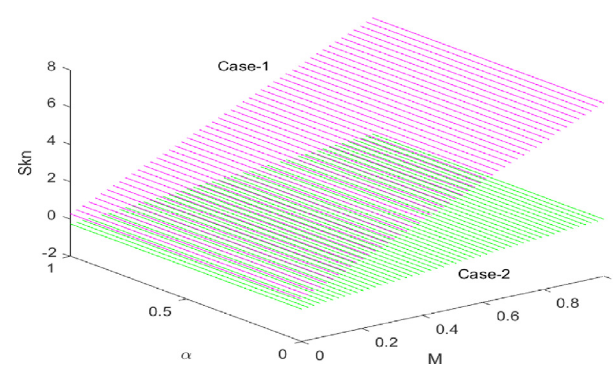

Fig. 10 The effect of M and α on Skn.

Case-1 Graphene (Cylindrical) + CNT(Spherical) + Alu minium oxide (Platelet) and.

Case-2 Copper oxide (Spherical) + Zirconium oxide (Cylindrical) + Magnesium oxide (Platelet).

The graphs Case-1 (Magenta) and Case-2 (Green) have the following colours. From Figs. 2 and 3, the effect of φ, φ_1 on Nu_x, we analyse that Case-1 contains more Nu_x rate of transmission in comparison to case-2;from Figs. 4 and 5, the impact of φ, φ_2 on Nu_x, we analyse that Case-1 have more Nu_x comparing the transfer rate to case-2,From Figs. 6 and 7 the impact of φ, φ_3 on Nu_x, we analyse that Case-1 has more

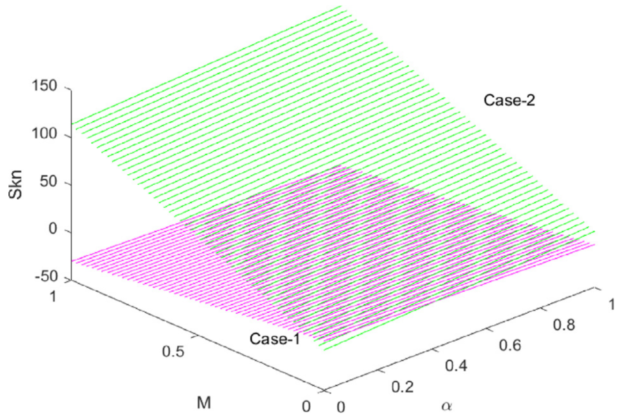

Fig. 11 The effect of α and M on Skn.

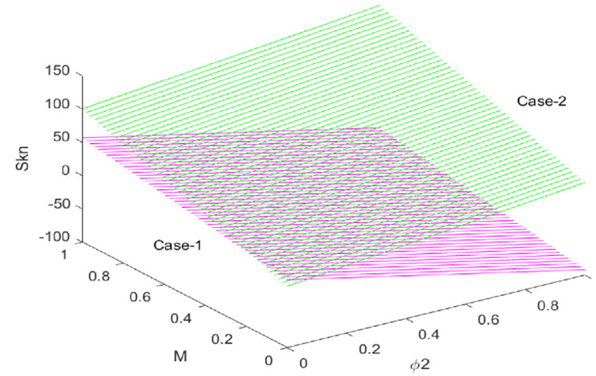

Fig. 14 The effect of φ_2 and M on Skn.

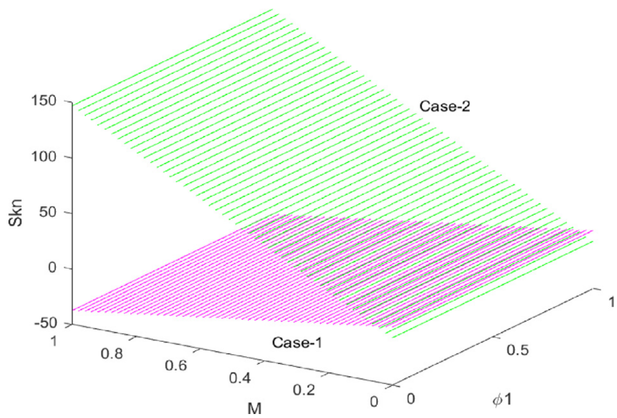

Fig. 12 The effect of φ_1 and M on Skin.

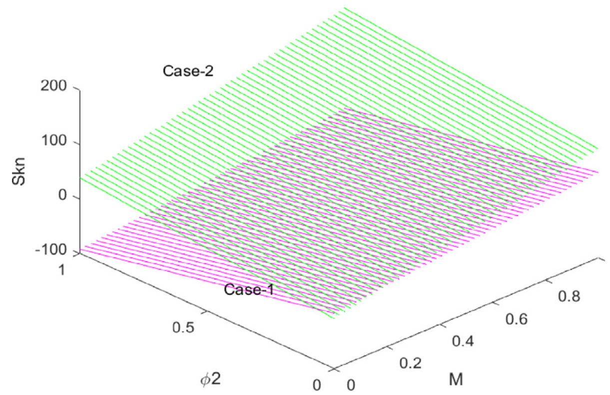

Fig. 15 The effect of M and φ_2 on Skn.

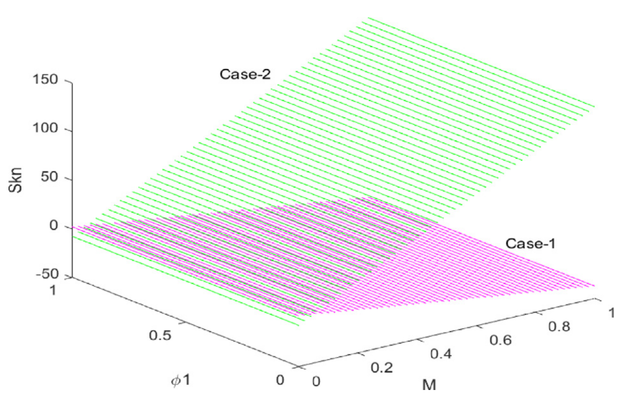

Fig. 13 The effect of M and φ_1 on Skn.

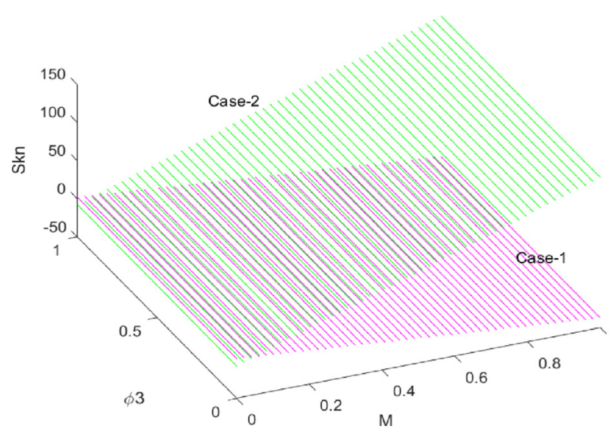

Fig. 16 The effect of M and φ_3 on Skn.

Nu_x comparing the transfer rate to case-2,From Figs. 8 and 9 the impact of Pr, b on Nu_x, we analyse that Case-1 entails more Nu_x rate of transmission in comparison to instance-2.Here we observed Case-1 having more Nu_x transfer rate than case-2 with different parameters effects also, it was happening due to the high density thermophysical properties of Case-1 Nanofluid particles. From Fig:10, the effect M, α on C_f, we analyse that Case-1 includes more numbers C_f in contrast to case-2 and from Fig. 11, we can observe that C_f Case 2 has a higher rate than Case 1 does. From Figs. 12 and 13, the effect M, φ_1 on C_f, we analyse that Case-2 includes more C_f rate as opposed to scenario-1.We can see the dominance of a magnetic parameter; from Figs. 14 and 15, the effect on C_f, we analyse that Case-2 includes more C_f rate compared to scenario-1. From Figs. 16 and 17, the effect M, φ_3 on C_f, we analyse that Case-2 includes more C_f rate compared to instance-1 and also, we can see the dominance of magnetic parameter.

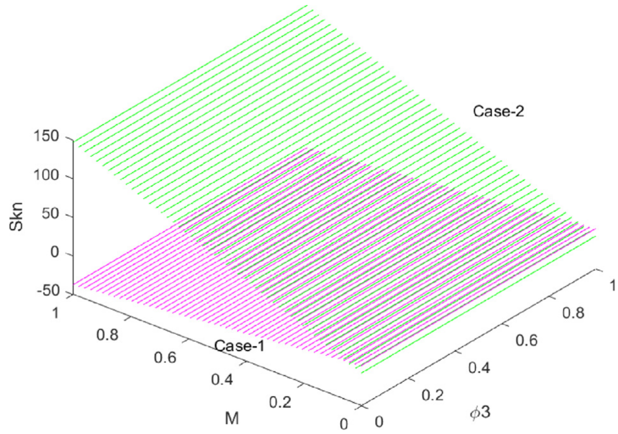

Fig. 17 The effect of φ_3 and M on Skn.

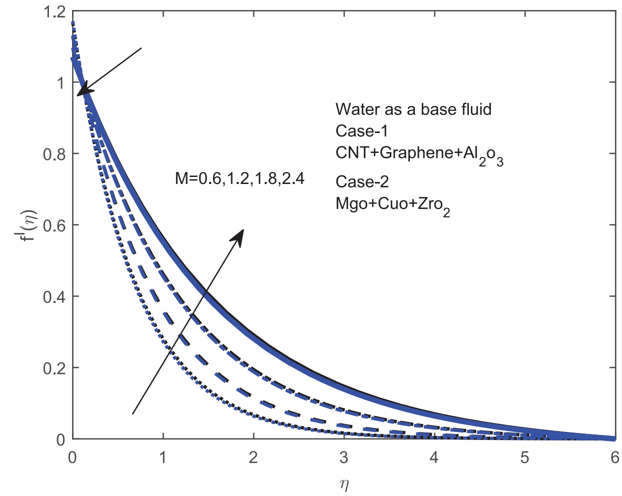

Fig. 20 Velocity outline for M.

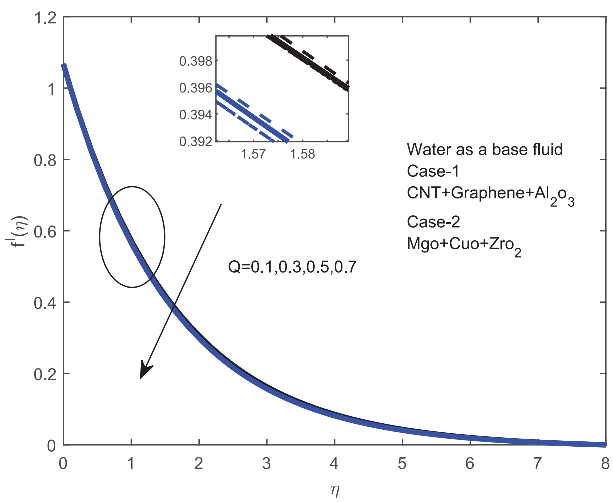

Fig. 18 Velocity outline for Q.

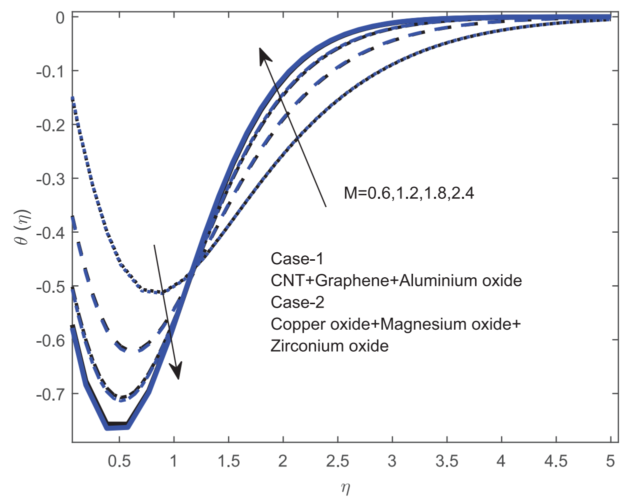

Fig. 21 Temperature outline for M.

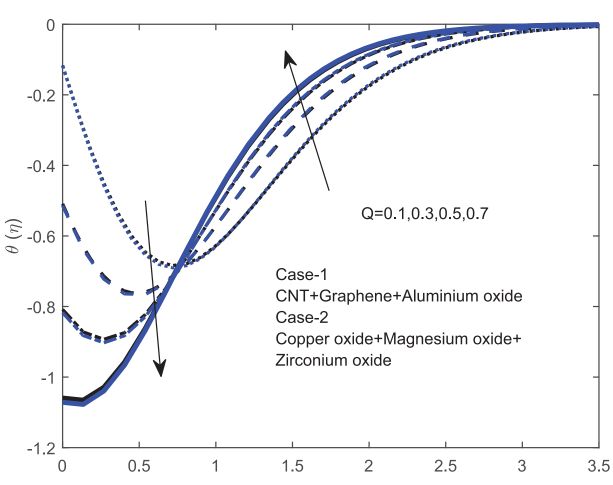

Fig. 19 Temperature outline for Q.

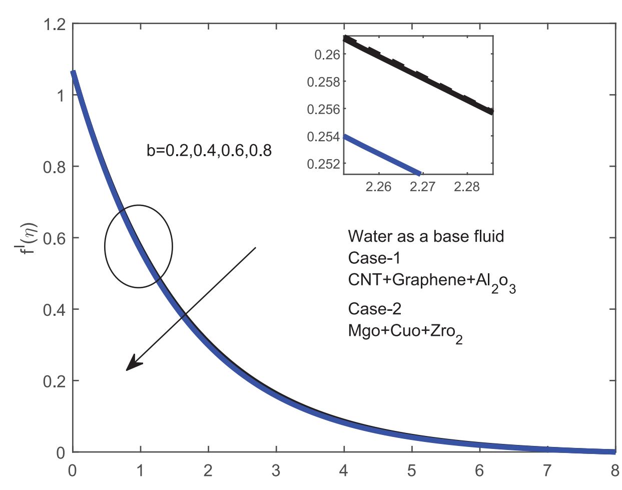

Fig. 22 Velocity outline for b.

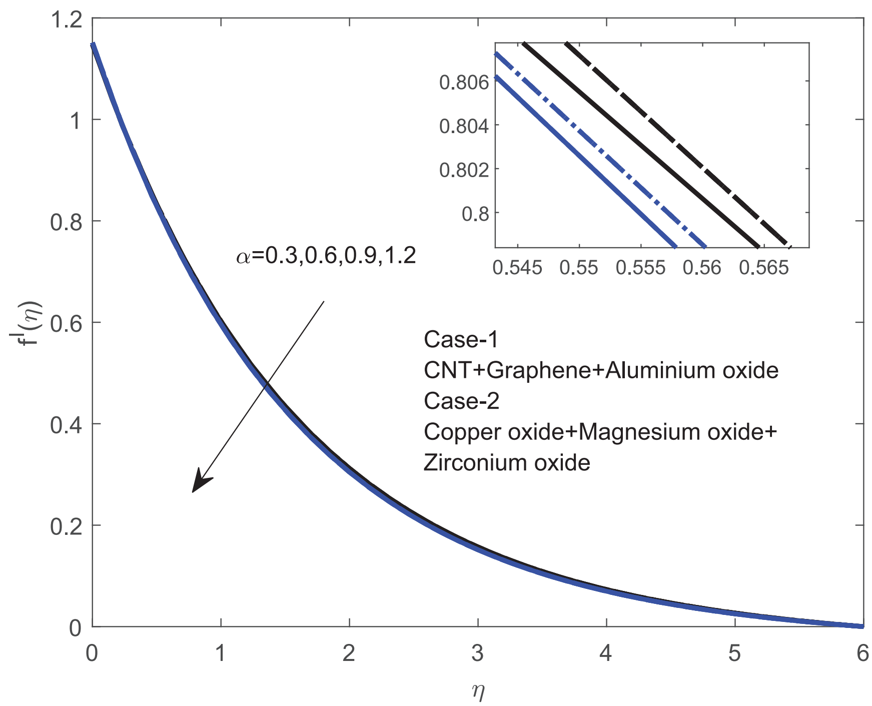

Fig. 23 Velocity outline for α.

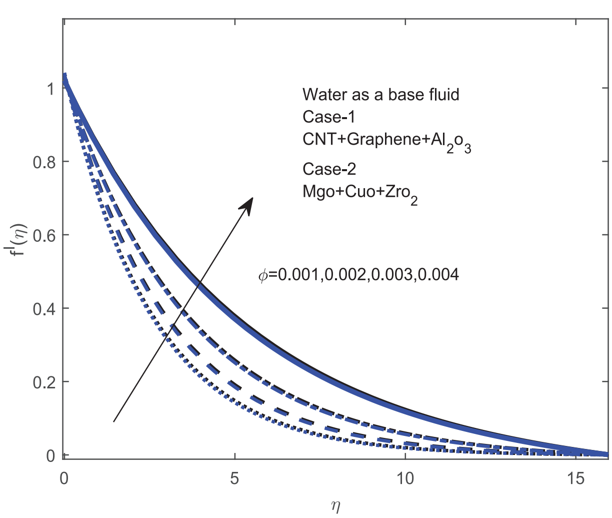

Fig. 24 Velocity outline for φ.

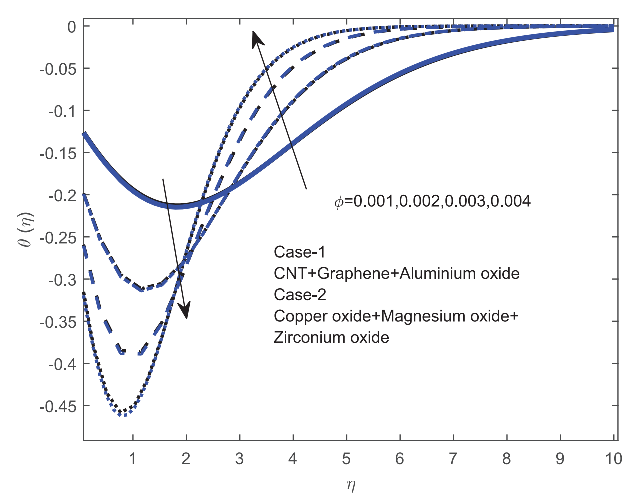

Fig. 25 Temperature outline for various values of φ.

In Table 2 In scenario 1, we can see that the Nusselt number transfer has a higher transmission rate. ($Al_2o_3 + GNT + CNT$ with water) than case-2 ($Mgo + Zro_2 + Cuo\ with\ water$),it indicates that Case-1 hybrid nanofluid mixture can be use where ever the higher heat transfer rate is required like fast charging batteries as well as for the cooling purpose due to their enhancement of heat transmission rate. Case-2 hybrid nanofluid mixture can be used where the less heat transfer rate is occurred than case-1.Even in cancer treatment also nanoparticles will be useful to kill the cancer cell by injecting the nanoparticles in to the human body.

The results demonstrate how dimensionless regulating factors like Volume fraction can be(φ), Heat sink/source (Q), Pr, M, b and α affect dimensionless Velocity and Temperature profiles (See Figs. 18-27). $M = 0.5, \varphi = 0.01, b = 0.1, \Pr = 6.2, Q = 0.5, \alpha = 0.2$ are the same values has been used in the entire problem; these values are same in the study, including the varies values are displayed in the tables and figures. Additionally, we used a table to display the C_f and Nu_x.

Figs. 18-27 illustrate the variations in the $f'(\eta), \theta(\eta)$ figures for various profiles $b = 0.1, \varphi = 0.01, M = 0.5, Q = 0.5, \alpha = 0.2$ and $\Pr = 6.2$. values. A heat sink, in general, is a passive heat exchanger that transfers heat from an electrical or mechanical equipment into a fluid that is flowing to cool the device. A heat source is anything that emits or creates heat. From Figs. 18 and 19, in our study we can study the influence

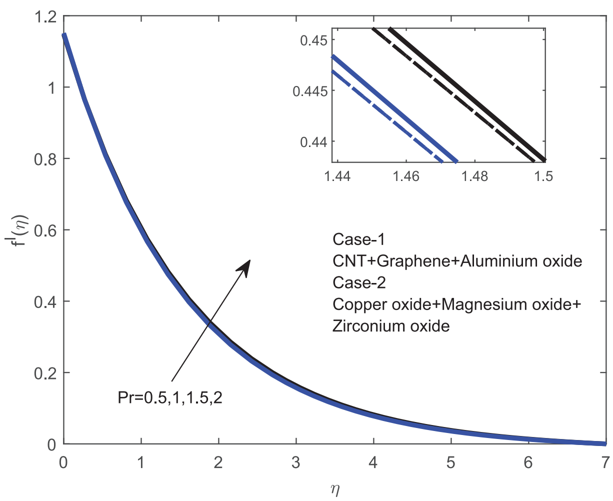

Fig. 26 Velocity outline for Pr.

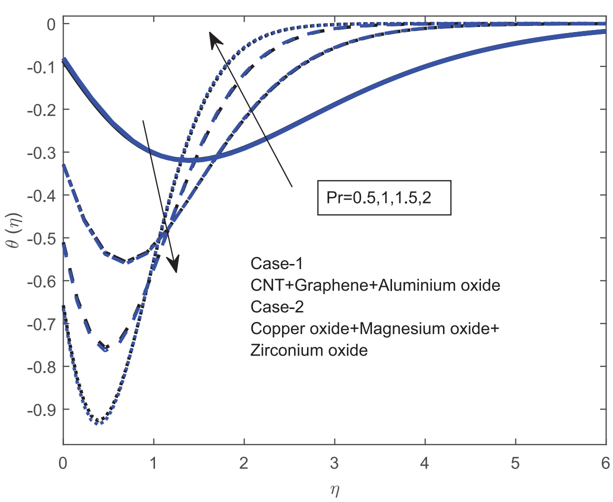

Fig. 27 Temperature outline for Pr.

of heat sink/source on velocity and temperature profiles figures. The velocity profile decreased when the Q raises, but in the temperature profile, we can observe reverse results up to $x = 0.80769$ and $y = 0.64242$. The curvature fell afterward, and curvature increased. When the magnetic parameter rises, the magnitude of the velocity profiles in the boundary layer often decreases, raising the temperature in the layer as a result. From Figs. 20 and 21, in our study we can keep the M effect on the temperature, velocity profiles figures; velocity profile decreases up to $x = 0.25641$ and $y = 0.97197$ afterward, velocity curvature rises than in temperature profile up to $x = 1.2821$ and $y = -0.44623$ after that raises the profile. Generally, at the boundary all the properties like velocity will be zero but when you applied slip condition those properties are non-zeros like velocity etc.

From Fig. 22, noticed the influence of a b –on velocity profile, Velocity curvature has been increasing, and the Temperature curvature profile has been increasing. The effect of velocity slip on the velocity profiles can be seen in Fig. 23; as the velocity increases, the curvature of the velocity profile diminishes while the temperature profile rises. In general, when the volume percentage of nanoparticles rises, velocity profiles rise while temperature values fall as heat transmission rises. From Figs. 24 and 25, in ours study we can notice the effect of φ on Temperature and Velocity profiles, velocity curvature raises when φ grows, and the temperature profile reduced at $x = 2.3077$ and $y = -0.2093$ afterward increasing. Prandtl number definition says that it is an ratio of Momentum diffusion and Thermal diffusion.it means velocity profile needs to increase when Prandtl number increases and will happen reverse behaviour in Temperature profile. From Figs. 26 and 27,in our study we can observe the effect of the Pr velocity profile has been increasing, based on temperature profiles and velocity profiles, When the Pr raises as we all see as the Temperature profile decreases up to $x = 1.3077$ and $y = -0.31336$ afterward temperature profile has been growing. Table 1 lists the thermophysical characteristics of nanoparticles based on their shapes, such as platelet, spherical, and cylindrical, with Cases-1 and 2 being CNT, graphene, and aluminium oxide and water, respectively. Using Table 2,when the Velocity slip raises, its effect on C_f is greater in case-2 compared to case-1,Local Nu_x raises in both cases when the velocity slip raises, but we can observe that the Nu_x transmission rate more in case-2 than compared to case-1. The impact of thermal slip C_f rate in case-2 is more than in case-1; the Local Nu_x rate increases when the thermal slip is rising. When the Hartman number rises, C_f in both cases also grows, but we can observe that case-2 has more C_f transmission rate than cae-1; when the M raises, we can keep the decreasing rate of the Nu_x in both cases. When the φ increases, we can reduce the C_f rate in both cases, which happens in the Nu_x. The effect of the Pr on the C_f rate, we can observe that in case-2 is more than in case-1, Nu_x rate is increasing in both the cases when Pr increases but we can keep that in case-1 having more transmission rate than case-2. The effect of heat source/sinks on C_f in case-2 is more than in case-1; when the Q raises, the Nu_x transmission rate declines (see Tables 3 and 4).

Table 1 Thermophysical properties of a Hybrid nanofluid.

	Nanoparticle shapes	Nomenclature of nano-particles and base fluid	ρ (kg/m^3)	Cp (J/kgK)	K (W/mK)
Base fluid		Water H_2O	997.1	4.179	0.623
Ternary hybrid Nanofluid 1	Cylindrical	Graphene	2200	5000	790
	Spherical	Carbon nanotubes	5100	410	3007
	Platelet	Aluminum oxide Al_2O_3	3970	765	40
Ternary hybrid Nanofluid 2	Cylindrical	Zirconium oxide	5680	502	1.7
	Spherical	Copper oxide	6500	535.6	20
	Platelet	Magnesium oxide	3560	955	45

Table 2 The physical parameter values for the local Nusselt number and the skin friction coefficient.

						Skin friction		Nusselt number	
α	b	M	φ	Pr	Q	Case-1	Case-2	Case-1	Case-2
0.3						2.910539	2.970850	1.761623	1.760235
0.6						2.910539	2.970850	2.119132	2.122485
0.9						2.910539	2.970850	2.658699	2.672473
1.2						2.910539	2.970850	3.566862	3.607149
	0.2					2.910539	2.970850	1.667832	1.665484
	0.4					2.910539	2.970850	1.866591	1.866417
	0.6					2.910539	2.970850	2.119132	2.122485
	0.8					2.910539	2.970850	2.450702	2.459991
		0.6				2.900501	2.968555	1.589243	1.585514
		1.2				3.970245	4.072791	1.367119	1.361601
		1.8				5.538076	5.692991	1.023637	1.015742
		2.4				7.536554	7.765449	0.583346	0.573340
			0.001			8.104846	8.242196	3.752479	3.715795
			0.002			5.554890	5.667601	2.861557	2.838495
			0.003			4.556270	4.655135	2.491804	2.472684
			0.004			3.989300	4.079176	2.252539	2.236433
				0.5		2.713453	2.780993	0.152805	0.139182
				1		2.713428	2.780966	0.063171	0.088891
				1.5		2.713454	2.780993	0.047499	0.077631
				2		2.713454	2.780993	0.161948	0.137534
					0.1	2.910539	2.970850	3.307496	3.304291
					0.3	2.910539	2.970850	2.518977	2.515988
					0.5	2.910539	2.970850	1.583524	1.580414
					0.7	2.910539	2.970850	0.376946	0.371636

Table 3 The regression statistics for Skin friction and Nusselt number.

Regression Statistics	Nusselt number	Skin friction
	Case-1,2	Case-1,2
Multiple R	1	1
R Square	1	1
Adjusted R Square	65,535	65,535
Standard Error	0	0
Observations	5	5

Table 4 Comparison of study the validity and reliability as follows.

	Akber et al. (Rasool et al., 2023)	Present results
$M = 1.5$	1.32288	1.32288
$M = 1$	1.18322	1.18322
$M = 0.5$	1.02472	1.02472

5. Conclusion

The scaling group Lie Group transformations was used, the influence of thermal slip and velocity slip with (THNF) Ternary hybrid nanofluids Case-1 CNT, Aluminium oxide and Graphene and case-2 Copper oxide, Magnesium oxide and Zirconium oxide with water as a base fluid and analysed the effect of parameters $Q, \Pr, \varphi, M, \alpha$ and b on rate of mass and heat transmission, Due to their increased thermal properties, hybrid nanofluids are frequently used as coolants in heat transmission equipment such electronic cooling, heat exchanger systems (like flat panel displays), and radiators. This study's findings revealed that:

We can see that instance-1 Nusselt number transfer has a higher transmission rate.($Al_2o_3 + GNT + CNT$ with water) than in case-2 ($Mgo + Zro_2 + Cuo$ *with water*), This shows that, due to the Case-1 hybrid nanofluid mixture's improved heat transmission rate, it can be used for cooling as well as other applications where a faster heat transfer rate is necessary, including rapid charging batteries. Where there is a lower heat transfer rate than in instance 1, the case-2 hybrid nanofluid mixture can be used. Even in cancer treatment also nanoparticles will be useful to kill the cancer cell by injecting the nanoparticles into the human body. In order to predict the outcomes of a response variable, a statistical technique known as multilinear regression analysis (MLR) makes use of a variety of explanatory variables.

- The hybrid nano fluid temperature profile raises, and the velocity profile falls when Q raised.
- The temperature and velocity characteristics of the hybrid nano fluid fluctuate when M is raised.
- The hybrid nano fluid temperature profile fluctuates and the velocity profile falls the when α is raised.
- The velocity profile and temperature profile of the hybrid nano fluid change, When b is raised.
- The temperature profile of the hybrid nano fluid changed, and the velocity profile rose, when φ raised.
- The velocity profile of the hybrid nano fluid increased while the temperature profile changed, when Pr is raised.

Future possible works:

The dual dynamical leaps on Lie group analysis of hydro-magnetic flow in a suspension of various forms of water-based hybrid solid particles with Fourier flux were taken into consideration in the current research.

1. Using different approximations, machine learning techniques like gradient descent approaches can be added and investigated.
2. By incorporating bio-convection into the model, this can be furthered.

3. Additionally, it can be expanded by incorporating various diffusivity qualities and linear as well as nonlinear porous layers (Triple diffusion).

Declaration of Competing Interest

The authors declare that they have no known competing financial interests or personal relationships that could have appeared to influence the work reported in this paper.

Acknowledgments

This project was supported by Researchers Supporting Project number (RSP2023R411), King Saud University, Riyadh, Saudi Arabia.

References

Abderrahmane, A., Qasem, N.A.A., Younis, O., Marzouki, R., Mourad, A., Shah, N.A., Chung, J.D., 2022. MHD Hybrid Nanofluid Mixed Convection Heat Transfer and Entropy Generation in a 3-D Triangular Porous Cavity with Zigzag Wall and Rotating Cylinder. Mathematics. 10 (5), 769.

Abel, Subhas, M., Siddheshwar, P.G., Mahesha, N., 2009. Effects of thermal buoyancy and variable thermal conductivity on the MHD flow and heat transfer in a power-law fluid past a vertical stretching sheet in a non-uniform heat source. Int. J. Non Linear Mech. 44 (1), 1–12.

Ahmadi, M.H., Mirlohi, A., Nazari, M.A., Ghasempour, R., 2018. A review of thermal conductivity of various nanofluids. J. Mol. Liq. 265, 181–188.

Akbar, N.S., Hayat, T., Nadeem, S., Obaidat, S., 2012. Peristaltic flow of a Tangent hyperbolic fluid in an inclined asymmetric channel with slip and heat transfer. Progress in Computational Fluid Dynamics, an International Journal 12 (5), 363–374.

Akbar, N.S., Nadeem, S., Haq, R.U., Khan, Z.H., 2013. Numerical solutions of magnetohydrodynamic boundary layer flow of tangent hyperbolic fluid towards a stretching sheet. Indian J. Phys. 87, 1121–1124.

Akinshilo, A.T., 2019. Thermal performance evaluation of MHD nanofluid transport through a rotating system undergoing uniform injection/suction with heat generation. BioNanoScience 9 (3), 740–748.

Akinshilo, A.T., 2020. Geometry shape effects of nanoparticles on fluid heat transfer through porous channel. AUT Journal of Mechanical Engineering 4 (1), 41–50.

Akinshilo, A.T., Ilegbusi, A., Ali, H.M., Surajo, A.J., 2020. Heat transfer analysis of nanofluid flow with porous medium through Jeffery Hamel diverging/converging channel. Journal of Applied and Computational Mechanics 6 (3), 433–444.

Akinshilo, A.T., Mabood, F., Ilegbusi, A.O., 2021. Heat generation and nonlinear radiation effects on MHD Casson nanofluids over a thin needle embedded in porous medium. Int. Commun. Heat Mass Transfer 127, 105547.

Akinshilo, A.T., Mabood, F., Badruddin, I.A., 2022. Thermal and entropy generation analysis of hybrid nanofluid flow through stretchable rotating system with heat source/sink. Waves Random Complex Media, 1–23.

Ali, A., Sarkar, S., Das, S., Jana, R.N., 2021. Investigation of cattaneo–christov double diffusions theory in bioconvective slip flow of radiated magneto-cross-nanomaterial over stretching cylinder/plate with activation energy. International Journal of Applied and Computational Mathematics 7 (5), 208.

Azhar, E., Iqbal, Z., Maraj, E.N., Ahmad, B., 2017. Influence of Cattaneo-Christov heat flux model on MHD hyperbolic tangent fluid over a moving porous surface. Frontiers in Heat and Mass Transfer (FHMT) 8.

Aziz, A., 2010. Hydrodynamic and thermal slip flow boundary layers with constant heat flux conditions over a flat plate. Commun. Nonlinear Sci. Numer. Simul. 15 (3), 573–580.

Aziz, Abdul. (2009). "A similarity solution for laminar thermal boundary layer over a flat plate with a convective surface boundary condition." Communications in Nonlinear Science and Numerical Simulation 14, no. 4 1064-1068.Hamad, M. A. A., Md J. Uddin, and AI Md Ismail.

Das, S., Sensharma, A., Jana, R.N., Makinde, O.D., 2017. Second-order slip flow of magneto-nanofluids along a stretching cylinder with prescribed heat flux. Journal of Nanofluids 6 (4), 720–727.

Das, S., Ali, A., Jana, R.N., 2021. Darcy-Forchheimer flow of a magneto-radiated couple stress fluid over an inclined exponentially stretching surface with Ohmic dissipation. World Journal of Engineering 18 (2), 345–360.

Friedman, A.J., Dyke, S.J., Phillips, B.M., 2013. Over-driven control for large-scale MR dampers. Innovative materials and structures 22, (4) 045001.

Huminic, G., Huminic, A., 2020. Entropy generation of nanofluid and hybrid nanofluid flow in thermal systems: a review. J. Mol. Liq. 302, 112533.

Investigation of combined heat and mass transfer by Lie group analysis with variable diffusivity taking into account hydrodynamic slip and thermal convective boundary conditions." International Journal of Heat and Mass Transfer 55, no. 4 (2012): 1355-1362.

Kashyap, S., Sarkar, J., Kumar, A., 2021. Effect of surface modifications and using hybrid nanofluids on the energy-exergy performance of the regenerative evaporative cooler. Build. Environ. 189, 107507.

Lie, S., 1891. Vorlesungen über differentialgleichungen: mit bekannten infinitesimalen transformationen. BG Teubner.

Mabood, F., Akinshilo, A.T., 2021. Stability analysis and heat transfer of hybrid Cu-Al2O3/H2O nanofluids transport over a stretching surface. Int. Commun. Heat Mass Transfer 123, 105215.

Makinde, O.D., Das, S., Jana, R.N., 2016. Effects of Navier Slip on MHD Chemically Reacting Nanofluid Over a Convective Permeable Surface with Radiative Heat. Journal of Nanofluids 5 (5), 687–695.

Martin, M.J., Boyd, I.D., 2006. Momentum and heat transfer in a laminar boundary layer with slip flow. J. Thermophys Heat Transfer 20 (4), 710–719.

Martin, M.J., Boyd, I.D., 2010. Falkner-Skan flow over a wedge with slip boundary conditions. J. Thermophys Heat Transfer 24 (2), 263–270.

Misra, J.C., Sinha, A., Shit, G.C., 2010. Flow of a biomagnetic viscoelastic fluid: application to estimate blood flow in arteries during electromagnetic hyperthermia, a therapeutic procedure for cancer treatment. Appl. Math. Mech. 31 (11), 1405–1420.

Mukhopadhyay, S., Layek, G.C., Samad, S.A., 2005. Study of MHD boundary layer flow over a heated stretching sheet with variable viscosity. Int. J. Heat Mass Transf. 48 (21–22), 4460–4466.

Naseer, M., Malik, M.Y., Nadeem, S., Rehman, A., 2014. The boundary layer flow of hyperbolic tangent fluid over a vertical exponentially stretching cylinder. Alex. Eng. J. 53 (3), 747–750.

Pakdemirli, M., 1992. Similarity analysis of compressible boundary layers for arbitrary profiles. Mech. Res. Commun. 19 (5), 399–406.

Pakdemirli, M., Yurusoy, M., 1998. Similarity transformations for partial differential equations. SIAM Rev. 40 (1), 96–101.

Rasool, G., Ahammad, N.A., Ali, M.R., Shah, N.A., Wang, X., Shafiq, A., Wakif, A., 2023. Hydrothermal and mass aspects of MHD non-Darcian convective flows of radiating thixotropic nanofluids nearby a horizontal stretchable surface: Passive control strategy. Case Studies in Thermal Engineering 42, 102654.

Raza, Q., Qureshi, M.Z., Khan, B.A., Kadhim Hussein, A., Ali, B., Shah, N.A., Chung, J.D., 2022. Insight into dynamic of mono and hybrid nanofluids subject to binary chemical reaction, activation energy, and magnetic field through the porous surfaces. Mathematics. 10 (16), 3013.

Reddy, M.G., Sudha Rani, M.V.V.N.L., Ganesh Kumar, K., Prasannakumar, B.C., Lokesh, H.J., 2020. Hybrid dusty fluid flow through a Cattaneo-Christov heat flux model. Physica A 551, 123975.

Sajjan, K., Shah, N.A., Ahammad, N.A., Raju, C.S.K., Kumar, M.D., Weera, W., 2022. Nonlinear Boussinesq and Rosseland approximations on 3D flow in an interruption of Ternary nanoparticles with various shapes of densities and conductivity properties. AIMS Mathematics 7 (10), 18416–18449.

Salahuddin, T., Malik, M.Y., Hussain, A., Awais, M., Khan, I., Khan, M., 2017. Analysis of tangent hyperbolic nanofluid impinging on a stretching cylinder near the stagnation point. Results Phys. 7, 426–434.

Sarkar, S., Jana, R.N., Das, S., 2020. Activation energy impact on radiated magneto-Sisko nanofluid flow over a stretching and slipping cylinder: entropy analysis. Multidiscip. Model. Mater. Struct. 16 (5), 1085–1115.

Shah, N.A., Ebaid, A., Oreyeni, T., Yook, S.-J., 2023. MHD and porous effects on free convection flow of viscous fluid between vertical parallel plates: advance thermal analysis. Waves Random Complex Media. https://doi.org/10.1080/17455030.2023.2186717.

Sivasankaran, S., Bhuvaneswari, M., Kandaswamy, P., Ramasami, E. K., 2006. Lie group analysis of natural convection heat and mass transfer in an inclined surface. Nonlinear Analysis: Modelling and Control 11 (2), 201–212.

Soltani, F., Toghraie, D., Karimipour, A., 2020. Experimental measurements of thermal conductivity of engine oil-based hybrid and mono nanofluids with tungsten oxide (WO3) and MWCNTs inclusions. Powder Technol. 371, 37–44.

Ullah, Z., Zaman, G., 2017. Lie group analysis of magnetohydrodynamic tangent hyperbolic fluid flow towards a stretching sheet with slip conditions. Heliyon 3 (11), e00443.

Upadhya, M.S., Raju, C.S.K., 2022. Implementation of boundary value problems in using MATLAB®. In: Micro and Nanofluid Convection with Magnetic Field Effects for Heat and Mass Transfer Applications Using MATLAB. Elsevier, pp. 169–238.

Younes, H., Mingyang Mao, S.M., Murshed, S., Lou, D., Hong, H., Peterson, G.P., 2022. Nanofluids: Key parameters to enhance thermal conductivity and its applications. Appl. Therm. Eng. 118202